Ceria-Supported Cobalt Catalyst for Low-Temperature Methanation at Low Partial Pressures of CO₂

Document license:
CC BY

DOI:
10.1002/anie.202214864

Document status and date:
Published: 26/01/2023

Document Version:
Publisher's PDF, also known as Version of Record (includes final page, issue and volume numbers)

Please check the document version of this publication:

• A submitted manuscript is the version of the article upon submission and before peer-review. There can be important differences between the submitted version and the official published version of record. People interested in the research are advised to contact the author for the final version of the publication, or visit the DOI to the publisher's website.
• The final author version and the galley proof are versions of the publication after peer review.
• The final published version features the final layout of the paper including the volume, issue and page numbers.

Link to publication

GDCh

Research Articles

Angewandte
Chemie
International Edition
www.angewandte.org

CO₂ Methanation | Hot Paper

Ceria-Supported Cobalt Catalyst for Low-Temperature Methanation at Low Partial Pressures of CO₂

Job J. C. Struijs, Valery Muravev, Marcel A. Verheijen, Emiel J. M. Hensen,* and Nikolay Kosinov*

Abstract: The direct catalytic conversion of atmospheric CO₂ to valuable chemicals is a promising solution to avert negative consequences of rising CO₂ concentration. However, heterogeneous catalysts efficient at low partial pressures of CO₂ still need to be developed. Here, we explore Co/CeO₂ as a catalyst for the methanation of diluted CO₂ streams. This material displays an excellent performance at reaction temperatures as low as 175 °C and CO₂ partial pressures as low as 0.4 mbar (the atmospheric CO₂ concentration). To gain mechanistic understanding of this unusual activity, we employed in situ X-ray photoelectron spectroscopy and operando infrared spectroscopy. The higher surface concentration and reactivity of formates and carbonyls —key reaction intermediates—explain the superior activity of Co/CeO₂ as compared to a conventional Co/SiO₂ catalyst. This work emphasizes the catalytic role of the cobalt-ceria interface and will aid in developing more efficient CO₂ hydrogenation catalysts.

Introduction

The atmospheric carbon dioxide concentration is increasing at an accelerating pace. Mitigation of the negative consequences from CO₂ emissions, i.e. climate change, is a significant challenge.[1] Carbon dioxide capture followed by its utilization via catalytic hydrogenationto useful chemical building blocks and fuels is a promising solution to this problem.[1, 2] Methane, being the most favored hydrogenation product thermodynamically, is a suitable molecule for CO₂ utilization.[3] High yields of methane can be achieved even under atmospheric pressure, in contrast to other hydrogenation products—methanol and higher hydrocarbons/oxygenates.[4, 5] Moreover, methane is compatible with the existing natural gas transport and distribution infrastructure.[6] Importantly, the methanation of CO₂ (Sabatier reaction) is a promising process for the storage of renewable energy[7] and the removal of CO$_x$ from hydrogen-rich streams (needed for ammonia production and fuel cells).[8] Lastly, methanation can be used to upgrade biogas streams to a high-quality synthetic natural gas by converting CO$_x$ and increasing the methane content.[6] The efficiency and practical applicability of all these processes depend on the activity, selectivity, and stability of methanation catalysts.

Many transition metals can catalyze CO₂ methanation. High activity and stability in a broad temperature range is achieved over costly noble metals (e.g., Ru and Rh).[4] More affordable and extensively studied Ni catalysts demonstrate a limited activity in low-temperature (< 200 °C) CO₂ methanation (Figure S1). Cobalt is an alternative base metal catalyst for the low-temperature methanation, although Co catalysts with high activity below 200 °C are yet to be identified (Figure S1). Furthermore, to date, numerous studies focused on the effect of increasing the reactant partial pressures on the performance of CO₂ catalysts.[9] On the contrary, the reaction at a low partial pressure of CO₂ remains largely underexplored, especially for heterogeneous systems (Figure S2).[10] This aspect is increasingly important for the direct valorization of atmospheric CO₂, with no separate energy-intensive separation and purification steps, which can offer environmental and economic benefits.[11, 12] Kuramoto and co-workers, for example, demonstrated the feasibility of such a process in a cycled fixed-bed reactor using a hybrid Ni/Na-γ-Al₂O₃ system, fulfilling both the roles of CO₂ adsorbent and methanation catalyst.[13]

Generally the activity and selectivity of methanation catalysts strongly depend on the support material and the nature of the metal-support interactions (MSI).[8, 14] For example, redox properties,[15] charge transfer effects,[16] and formation of metal-support interfacial sites[3, 17] were reported to influence the catalytic performance of methanation catalysts. Catalysts supported by the redox-active cerium dioxide (CeO₂, ceria) are particularly active in CO₂ methanation.[18, 19] The abundant basic sites in addition to the

[*] J. J. C. Struijs, V. Muravev, E. J. M. Hensen, N. Kosinov
Laboratory of Inorganic Materials and Catalysis, Department of Chemical Engineering and Chemistry Eindhoven University of Technology
P.O. Box 513, 5600MB Eindhoven (The Netherlands)
E-mail: E.J.M.Hensen@tue.nl
        N.A.Kosinov@tue.nl

M. A. Verheijen
Department of Applied Physics Eindhoven University of Technology
P.O. Box 513, 5600MB Eindhoven (The Netherlands)
and
Eurofins Material Science Netherlands BV
5656AE Eindhoven (The Netherlands)

high reducibility of ceria, easily forming oxygen vacancies, were reported to result in a strong adsorption and subsequent activation of CO_2.[20] Recently we demonstrated how the performance of ceria-based catalysts can be optimized through engineering of the Co-CeO_2 interface.[8]

In this work, we demonstrate that Co/CeO_2 can efficiently catalyze low-temperature CO_2 methanation at low partial pressures of CO_2. Co/CeO_2 displays a high CO_2 methanation activity at CO_2 partial pressures as low as 0.4 mbar (corresponding to the atmosphere concentration of 400 ppm). Using transient kinetic step-response and steady-state isotopic transient kinetic analysis (SSITKA), followed by Fourier-transform infrared (FTIR) spectroscopy, we identified formate and carbonyl species as the key reaction intermediates. Operando FTIR spectroscopy demonstrated the presence of two types of formate species on Co/CeO_2. Both formates contribute to the formation of carbonyls but with a different rate. Furthermore, an additional linear carbonyl species, assigned to the adsorption of CO next to adsorbed carbon atoms, was identified. Lastly, the formation of oxygen vacancies and cerium hydrides during the reduction process of Co/CeO_2 was observed by near-ambient pressure X-ray photoelectron spectroscopy (NAP-XPS). The combination of higher reactivity of formates and carbonyls and the higher concentration of formates on Co/CeO_2, as compared to a reference Co/SiO_2 catalyst, explains the high activity of the ceria-based catalyst at a low partial pressure of CO_2 and low temperature. The mechanistic findings of this work emphasize and clarify the role of the cobalt-ceria interface and will help developing better catalysts for CO_2 hydrogenation.
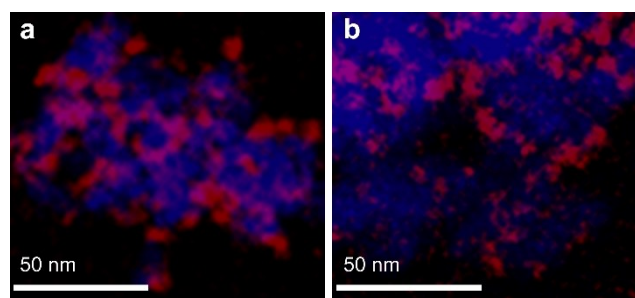

Figure 1. TEM-EDX mapping of a) Co/CeO_2 and b) Co/SiO_2. Cobalt particles are shown in red; the support in blue.

Results and Discussion

CO_2 Hydrogenation Activity of Co/CeO_2

A Co/CeO_2 and a Co/SiO_2 catalyst (9 wt %, Table S2) were prepared by strong electrostatic adsorption of an in situ formed hexaamminecobalt(III) complex ($[Co(NH_3)_6]^{3+}$) in wet impregnation mode. After calcination and reduction, the metal particle sizes for both catalysts were close to 7 nm, according to TEM and CO chemisorption (Table S2 and Figure S3). The even distribution of Co over both supports was confirmed by TEM-EDX (Figure 1).

After in situ reduction in hydrogen at 500 °C, the catalytic performance of the cobalt nanoparticles deposited on a reducible (CeO_2) and non-reducible (SiO_2) support was assessed (Figure 2). The catalytic activity was tested as a function of temperature at a low CO_2 partial pressure of 0.4 mbar (Figure 2a). Co/CeO_2 demonstrates a significantly higher activity than Co/SiO_2 at each temperature. Additionally, the prepared Co/CeO_2 catalyst demonstrates a higher
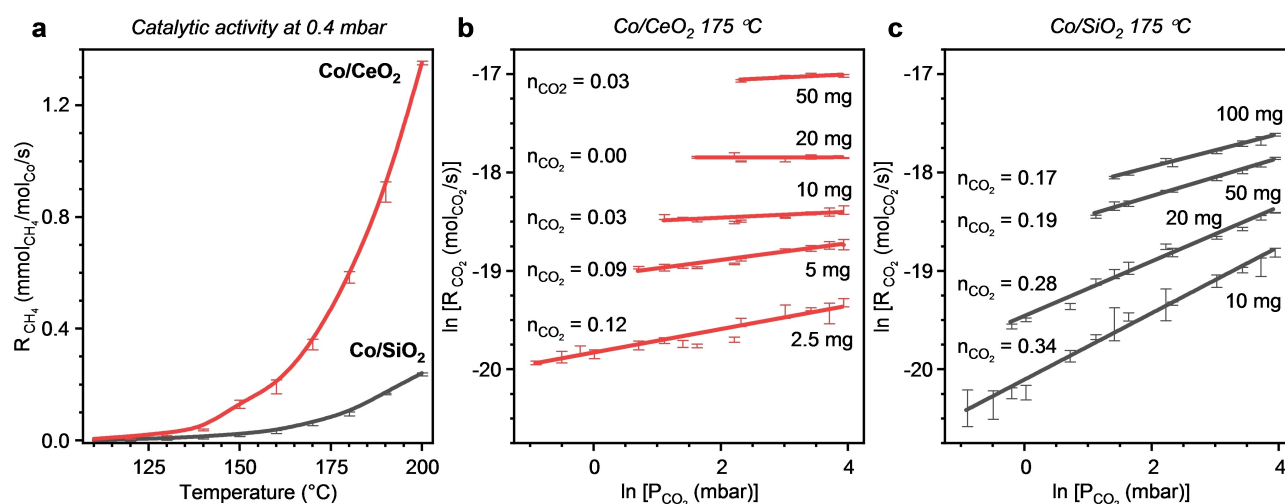
Figure 2. The catalytic activity of Co/CeO_2 and Co/SiO_2 in CO_2 hydrogenation. a) Rate of CH_4 formation as a function of temperature at 0.4 mbar of CO_2. Error bars indicate the standard deviation of measurements with different catalyst loadings (CO_2 conversions < 30 %). b), c) Reaction orders with respect to CO_2 (n_{CO_2} ±0.01) for Co/CeO_2 (b) and Co/SiO_2 (c) at 175 °C with CO_2 partial pressures of 0.4–5 mbar. The data of b&c expressed as specific reaction rates can be found in Figure S4. Error bars indicate the standard deviation between GC measurements (CO_2 conversions < 10 %, except 2.5 mg Co/CeO_2 at 400 ppm). Conditions: 2.5–100 mg catalyst, 0.4–5 mbar CO_2 and 200 mbar H_2 in He, total flow 200 mL min^{-1}.

low-temperature ($<200\,°C$) catalytic activity than previously reported Co and Ni catalysts (Figure S1).

In order to understand the difference in CO_2 activation between the studied catalysts, the reaction orders with respect to CO_2 were determined at $175\,°C$ (Figure 2b,c). The partial pressure of CO_2 was varied by two orders of magnitude—from 0.4 to 50 mbar. Over the whole pressure range, the Co/CeO_2 catalyst displays a much higher metal-normalized activity compared to Co/SiO_2 and previously reported Co and Ni catalysts (Figure S2). The methanation at low partial pressures of CO_2 over Co/CeO_2 proceeds with $>95\,\%$ selectivity to CH_4 (Figure S5). Under the same reaction conditions, the CH_4 selectivity over Co/SiO_2 was much lower. Interestingly, the reaction order in CO_2 is higher for Co/SiO_2 (Figure 2b,c). The near zero reaction orders for Co/CeO_2 demonstrate that the coverage of CO_2 during steady-state reaction is sufficiently high in the whole pressure range. This finding is in line with the ability of the CeO_2 support in efficiently capturing CO_2 from dilute streams.[20]

Operando FTIR Spectroscopy at Low and High Partial Pressures of CO_2

The activity of heterogeneous catalysts is governed by the transformation of surface intermediates.[14] To investigate the surface species present on the Co/CeO_2 and Co/SiO_2 catalysts during CO_2 methanation, operando FTIR spectroscopy was applied. Similar to the activity measurements, the experiments were performed at $175\,°C$ under steady-state conditions, as confirmed by mass spectrometry and FTIR (e.g., Figures S6, S7). The catalysts were reduced in H_2 at $500\,°C$ and subsequently exposed to a continuous flow of CO_2+H_2 ($200\ mL\,min^{-1}$) with either a high (25 mbar) or low (0.6 mbar) CO_2 partial pressure at $175\,°C$.

At both partial pressures (Figure 3), the characteristic bands located between $1700–2100\ cm^{-1}$ can be assigned to carbonyls adsorbed on metallic cobalt (*CO).[21] Bands centered at $\approx 1950\ cm^{-1}$ and higher are assigned to linear adsorption of CO (top-CO).[22] Bands located below $\approx 1950\ cm^{-1}$ are assigned to the bridged and hollow adsorption modes of CO (bridged-CO and hollow-CO).[21,23] Two different C–O stretch vibrations assigned to formate species were observed between $1550–1640\ cm^{-1}$ (C–O stretch I) and $1360–1390\ cm^{-1}$ (C–O stretch II). The C–H stretch ($2800–2890\ cm^{-1}$) and O–C-H bending ($\approx 1320–1370\ cm^{-1}$) formate vibrations were also identified.

Bicarbonates and multiple carbonate species were present on Co/CeO_2 as manifested by several bands in the regions of $1200–1650\ cm^{-1}$ and $950–1100\ cm^{-1}$ (Figure 3a).[3,24] The much higher surface coverages of formates, bicarbonates, and carbonates compared to Co/SiO_2 confirm the ability of ceria to strongly adsorb CO_2.[4] Previously, it was proposed that these species are the precursors that lead to the formation of carbonyl species and eventually methane formation on alumina- and ceria-supported catalysts.[3,25]

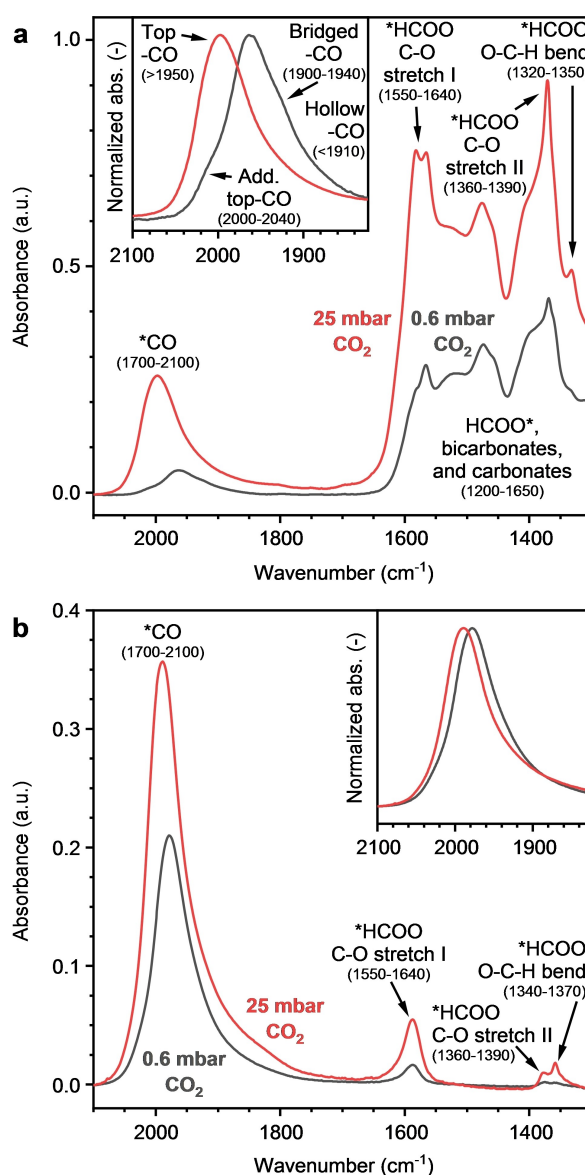The observed difference in the concentration of surface species at 0.6 and 25 mbar (Figure 3, discussed in Note S1)

Figure 3. Steady-state FTIR spectra at 0.6 mbar and 25 mbar CO_2 for a) Co/CeO_2 and b) Co/SiO_2. Several vibrations are indicated, including their approximate positions in cm^{-1}. The insets show the intensity-normalized carbonyl signals. All spectra were normalized by pellet weight. Conditions: $175\,°C$, 0.6 or 25 mbar $CO_2/200$ mbar H_2 in He, total flow $200\ mL\,min^{-1}$.

indicates the importance of studying the catalysts under the relevant reaction conditions, in this case low CO_2 partial pressure.[26] At 0.6 mbar of CO_2, an additional top-CO peak is observed as a blue-shifted shoulder at $2000–2040\ cm^{-1}$ (insets Figure 3), whereas at 25 mbar this peak could not be distinguished. Carbonyls are generally considered to be the key intermediate species for CO_2 methanation.[25] The recent work of Mansour and Iglesia emphasizes the pivotal role of carbonyls in methanation of both CO and CO_2.[27] In the next section we will focus on the evolution of surface carbonyls and the involvement of the $Co-CeO_2$ interface in the activation of CO_2.

Probing Oxidation, Carburization, and Hydridization of Co/CeO₂

To investigate the nature of the carbonyl species, CO-FTIR experiments were performed at 50 °C on reduced Co/SiO₂ and Co/CeO₂ samples. Based on time- and pressure-dependent CO adsorption experiments (Figure 4a,b, Note S2, and Figures S8–S13), the appearance of the blue-shifted carbonyl band around 2047 and 2057 cm⁻¹ for Co/CeO₂ and Co/SiO₂, respectively, can be explained by the adsorption of CO on sites adjacent to C_{ads} or O_{ads} atoms formed during CO dissociation.[23,28] The presence of C_{ads} and O_{ads} on the surface is corroborated by the evolution of gaseous CO_2 (formed via the Boudouard reaction) over both catalysts. In situ formation of CO_2 also led to the appearance of carbonate, bicarbonate, and formate bands (1650–1200 cm⁻¹, Figure 4a) on Co/CeO₂.[3,24] An alternative explanation for the observed blue-shifted carbonyl band is a partial oxidation of the cobalt surface by adsorbed oxygen atoms (O_{ads}).[21,29] We note that both explanations are in line with the time-dependent evolution of the additional carbonyl band upon exposure to 0.5 mbar of CO (Figure 4a,b), as the adsorbed species are formed during the exposure to CO.
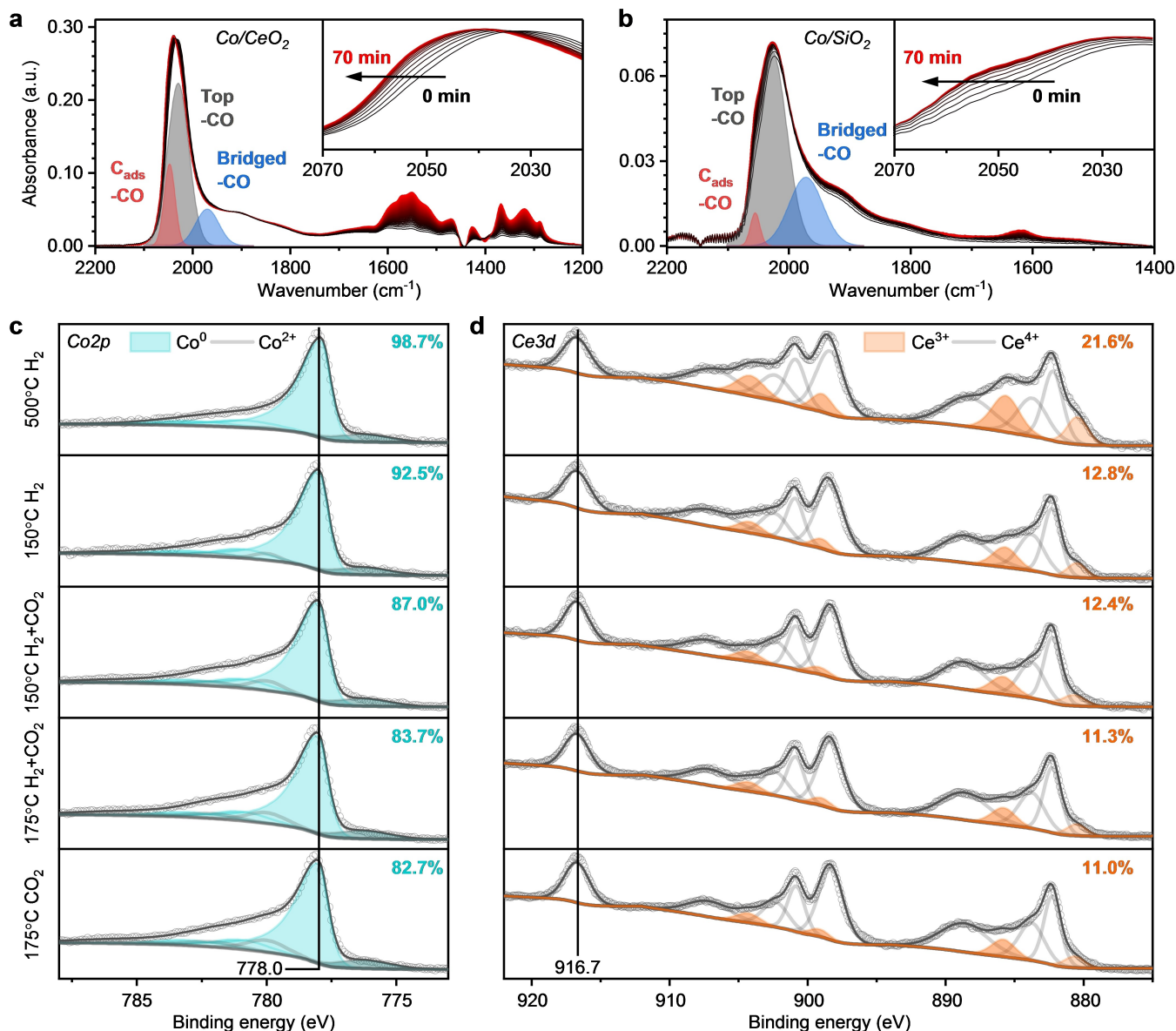
Figure 4. Surface behavior of Co/CeO₂ and Co/SiO₂. a), b) Time-dependent CO adsorption FTIR experiment over the course of 70 min after dosing 0.5 mbar CO (at $t=0$ min) on Co/CeO₂ (a) and Co/SiO₂ (b). The deconvoluted peaks for the blue-shifted CO species (C_{ads}-CO), top-CO and bridged-CO at $t=70$ min are shown. A full description and spectra for 0.1 mbar can be found in Note S2. The absorbance for each spectrum was background corrected and normalized by pellet weight. Conditions: 50 °C, 4 h reduction in H₂ at 500 °C. c), d) In situ lab-based NAP-XPS study of Co/CeO₂. c) Co 2p region (grey area corresponds to Co LMM Auger contributions). d) Ce 3d region. The top row was acquired after reduction at 500 °C in H₂. The catalyst was subsequently cooled down in hydrogen and exposed to different temperatures and gas compositions.

The possibility of the partial surface oxidation of Co/CeO$_2$ by O$_{ads}$ was investigated by in situ NAP-XPS experiments. To follow the oxidation state of cobalt and ceria upon exposure to CO, the percentage of Co^0 and Ce^{3+} were determined from the Co 2p and Ce 3d core line spectra, respectively. After treatment in hydrogen (1 mbar) at 500 °C, the Co$_3$O$_4$ precursor was completely reduced (Figure S14–S15). Additionally, the concentration of reduced Ce^{3+} species increased by ≈20 %, in line with the hydrogen temperature-programmed reduction results (Figure S16). Following the procedure of the FTIR experiment, the cell was evacuated to a high vacuum (10^{-8} mbar) at 500 °C and then cooled down to 50 °C. Upon exposing the sample to CO, no significant oxidation of cobalt was observed. Although lab-based NAP-XPS does not provide the utmost surface sensitivity (inelastic mean free path of Co 2p photoelectrons is ≈15 Å), we infer that these results disfavor the hypothesis of the partial oxidation of the cobalt surface by O$_{ads}$. The observed slight oxidation of Ce^{3+} (18.7 % to 16.8 % Ce^{3+}) under the same conditions (Figure S14b), however, indicates the dissociation of CO. In this process, C$_{ads}$ remains on the Co surface while O$_{ads}$ oxidizes the CeO$_2$ support via oxygen spillover or reacts with *CO to form CO$_2$ as observed by FTIR (Note S2).[8] Thus, the additional carbonyl peak in FTIR around 2047 cm^{-1} (subsequently referred to as C$_{ads}$-CO) is likely caused by the carburization of the cobalt surface.

Next, the redox behavior of cobalt and ceria under reaction conditions was investigated by exposing the reduced catalyst to a reaction mixture with 0.2 mbar CO$_2$ and 0.8 mbar H$_2$ at 150 °C and 175 °C (Figure 4c,d). After pretreatment, cobalt was fully reduced (top row Figure 4c) and ceria was substantially reduced (21.6 % Ce^{3+}, top row Figure 4d). Instead of cooling down in vacuum, as in the previous experiment, the sample was cooled down in hydrogen to 150 °C as during the activity tests. Counterintuitively, the presence of hydrogen during cooling resulted in a significant decrease of the Ce^{3+} concentration to 12.8 %. The apparent oxidation of Ce^{3+} to Ce^{4+} can be explained by the formation of cerium hydride species (Ce^{4+}H$^-$, Note S3).[30,31] Consistent with these results, the oxidation of Ce^{3+} continued during further cooling to 50 °C in the presence of H$_2$ (9.3 % Ce^{3+}, Figure S18). Oxidation of cobalt (+6.2 % Co^{2+}) observed by NAP-XPS upon cooling to 150 °C in H$_2$ (Figure 4c) can be linked to a reverse oxygen spillover at the cobalt-ceria interface, pointing to the strong interaction between cobalt and ceria.[8,32] Exposing the catalyst to reaction conditions (H$_2$+CO$_2$) leads to a gradual oxidation of the Co particles (Figure S19). At 150 °C we observed 87.0 % of Co^0 which decreased to 83.7 % of Co^0 at 175 °C (Figure 4c). Removing H$_2$ from the reaction mixture at 175 °C resulted only in a minimal further oxidation (82.7 % Co^0). Under reaction conditions ceria undergoes slight oxidation (Figure 4d) due to the filling of oxygen vacancies.[8,33]

Altogether, we conclude that both Co and CeO$_2$ participate in the activation of CO$_2$. Activation of CO$_2$ at the Co-CeO$_2$ interface under reaction conditions involves time- and temperature-dependent partial oxidation of both Ce^{3+} and Co^0. With this better understanding of the active site speciation, we focus in on operando FTIR spectroscopy to monitor the reaction intermediates.

Steady-State Operando FTIR Spectroscopy

Operando FTIR spectroscopy experiments were performed between 125 and 185 °C with a CO$_2$ partial pressure of 0.6 mbar to investigate the influence of temperature on the steady-state behavior of various surface species (Figure 5). The area of carbonyl signal strongly decreased between 125 and 185 °C on Co/CeO$_2$ (Figure 5a). The decrease in the total amount of carbonyls can primarily be ascribed to the decrease in linear carbonyls (Figure 5b). For top-CO, a significant red shift from 1975 to 1963 cm^{-1} and decrease in the peak area were observed from 145 °C onwards. The red shift is most likely caused by the decrease in *CO coverage and thereby a decrease in lateral carbonyl-carbonyl interactions, as observed in previous CO adsorption experiments (Note S2).[21] In contrast to linear carbonyls, multibonded carbonyls were more stable over the investigated temperature range—their quantity started decreasing significantly only above 165 °C. We note that Meunier and co-workers demonstrated that for CO hydrogenation on a Co/Al$_2$O$_3$ catalyst these multibonded carbonyls were the main reaction intermediates under the applied reaction conditions.[34]

The ceria-based catalyst contained two types of formates, one with a C–O stretch I vibration band at 1584 cm^{-1} and one at 1565 cm^{-1} (Figure 5c). In the C–H stretching vibration region, two contributions were observed as well (≈2855 and ≈2838 cm^{-1}, Figure 5d).[24] Moreover, two bands at 1369 and 1359 cm^{-1} were assigned to the C–O stretch II vibration. Using 2D correlation spectroscopy and H/D exchange experiments (Note S4 and Figures S22–S25), we found that peaks located at 2855, 1584, and 1369 cm^{-1} correspond to one formate species (formate-I) and peaks located at 2838, 1565, and 1359 cm^{-1} to another formate species (formate-II). Two types of formates were also reported previously for Ru/Al$_2$O$_3$,[35] Ru/TiO$_2$,[36] and Co/silica-alumina catalysts.[23] The total amount of formates decreased steadily from 145 °C to 185 °C (Figure 5b). Formate-I was only present to a minor extent at higher temperatures. The intensity of the carbonate bands, present in the same wavenumber range as the formate C-O stretch bands, strongly decreased above 145 °C.

In striking contrast to Co/CeO$_2$, the area of the carbonyl peaks on previously reported catalysts and Co/SiO$_2$ (Figure 5e) increased within the studied temperature range.[3,15,22,25,37] Deconvolution showed that the intensity of C$_{ads}$-CO remained approximately constant, while the other carbonyls contribute to the increase of the total peak area (Figure 5f). The total carbonyl amount increased by ≈20 % from 125 °C to 185 °C. Over the same temperature range, the area of the carbonyl peaks decreased by ≈50 % on Co/CeO$_2$. In line with the catalytic data, the different trend demonstrates that Co/CeO$_2$ is active for CO$_2$ dissociation at a much lower temperature compared to other catalysts. We should note that on Co/SiO$_2$ the position of the carbonyl
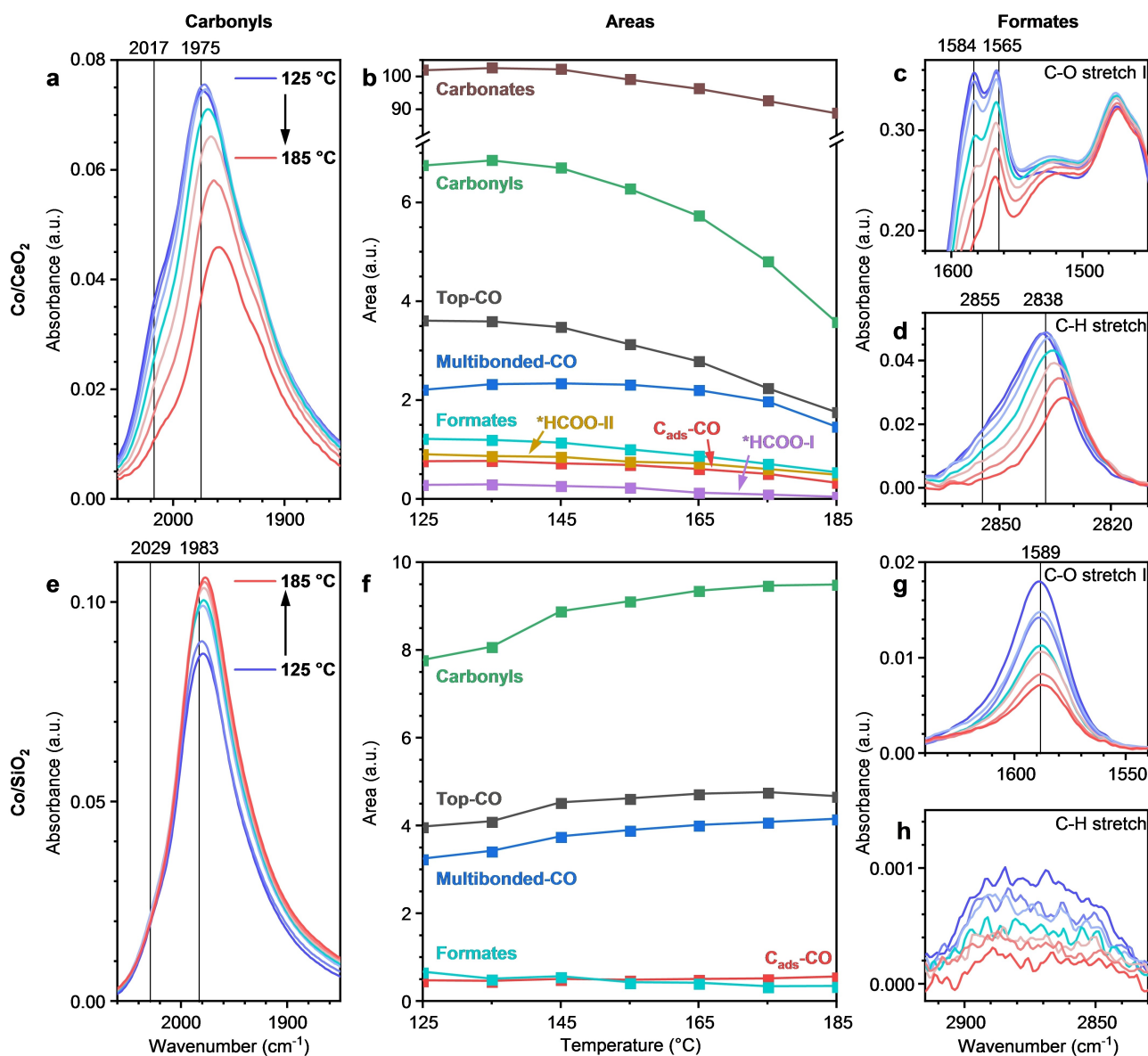
Figure 5. Temperature-resolved operando FTIR for Co/CeO$_2$ (a–d) and Co/SiO$_2$ (e–h) under steady-state conditions at 0.6 mbar of CO$_2$. a), e) Carbonyl region including the positions of C$_{ads}$-CO and top-CO at 125 °C. b), f) Peak area evolution over temperature obtained by deconvolution of the spectra. For the formates, the C−O stretch-I area is used. c), g) Formate C−O stretch region. d), h) Formate C−H stretch region. The lines indicate the positions of the formate species at 125 °C. Entire scans are provided in Figures S20 (Co/CeO$_2$) and S21 (Co/SiO$_2$). All spectra and areas are normalized by pellet weight. Conditions: 0.6 mbar CO$_2$ and 200 mbar H$_2$ in He, total flow 200 mL min^{-1}, 125–185 °C.

band was found at higher wavenumbers than on Co/CeO$_2$ at all temperatures. The higher wavenumbers might indicate a weaker bonding of the carbonyls to Co/SiO$_2$.[38] The lower bonding strength can contribute to the differences in the observed catalytic performance. For instance, the lower bonding strength can lead to the higher CO selectivity of Co/SiO$_2$ (Figure S5).[39]

Similar to Co/CeO$_2$, the intensity of the formate bands on Co/SiO$_2$ decreased over temperature (Figure 5g,h). Wang et al. also reported a decrease in formate intensity on Pd/Al$_2$O$_3$ at an increasing temperature.[25] The decreasing area of the formate peaks in combination with the increasing carbonyl peaks over temperature on Co/SiO$_2$ might indicate

that the formates decompose into carbonyls in the catalytic cycle.[25] In this scheme, the rate of formate decomposition increases with temperature, whereas the conversion of *CO to CH$_4$ is still slow. An alternative possibility is that formates do not play an important role in the mechanism and remain mere spectators.[40] To clarify the catalytic role of the surface intermediates and to further elucidate the properties of the different formate species on Co/CeO$_2$, next we performed operando FTIR under transient conditions.

Transient Operando FTIR Spectroscopy

Spectroscopic analysis of surface coverages during transient kinetic experiments is a powerful tool to reveal the mechanistic peculiarities of catalytic reactions.[41] In the transient kinetic step-response experiments of this work, the feed flow was rapidly switched from $CO_2/H_2/He$ to H_2/He while the response of the adsorbed species was monitored by acquiring time-resolved FTIR spectra. The intensity of all bands on both catalysts decreased after the switch (Figure 6). For Co/SiO_2, the intensity decays fast in the first five minutes (gray lines in Figure 6a) and after that the decay slows down. After 15 minutes, a small fraction of both the formates and carbonyls (23% and 9%, respectively, at 155°C) was still present on the Co/SiO_2 surface. The reaction temperature governs the response of the surface species. For example, at 125°C a large fraction of the carbonyls (66%) and formates (55%) was not removed from Co/SiO_2 after 15 minutes (Figure S26a–c). In contrast, almost no carbonyls and formates remained on the surface after 15 minutes at 185°C. Both carbonyl and formate species are significantly more dynamic on Co/CeO_2 and decompose faster at all temperatures.

To compare the transient behavior of different species at different temperatures, the band intensities were normalized (Figure 6b). Herein, the absorbance of the species of interest under steady-state reaction conditions is taken as unity and the absorbance before the feed was switched as zero. The time scale at which the formates and carbonyls are decomposed or hydrogenated is similar (Figure 6b), in line with a methanation mechanism involving both species.[25] The formate species on Co/SiO_2 display a fast initial decomposition rate followed by a period of slower decomposition (Figure 6b and Figure S27). A possible explanation for the fast and slow components could be the presence of different unresolved formate species on Co/SiO_2 (akin to the two formates observed on Co/CeO_2).[35,36,42] A certain degree of peak asymmetry observed for the formate C–O (1589 cm^{-1}) and C–H (2830–2910 cm^{-1}) stretch vibrations on Co/SiO_2 supports this explanation (Figure 6a and Figure 5g,h). Other possible explanations are a change of the catalyst surface related to varying surface coverages or a slight reduction of the cobalt surface after the switch to pure hydrogen.[21,23] The apparent decomposition rates were determined by fitting slopes to the normalized decay just after the feed was rapidly switched (indicated in red in Figure 6b,e). In this manner, the surface coverages are still
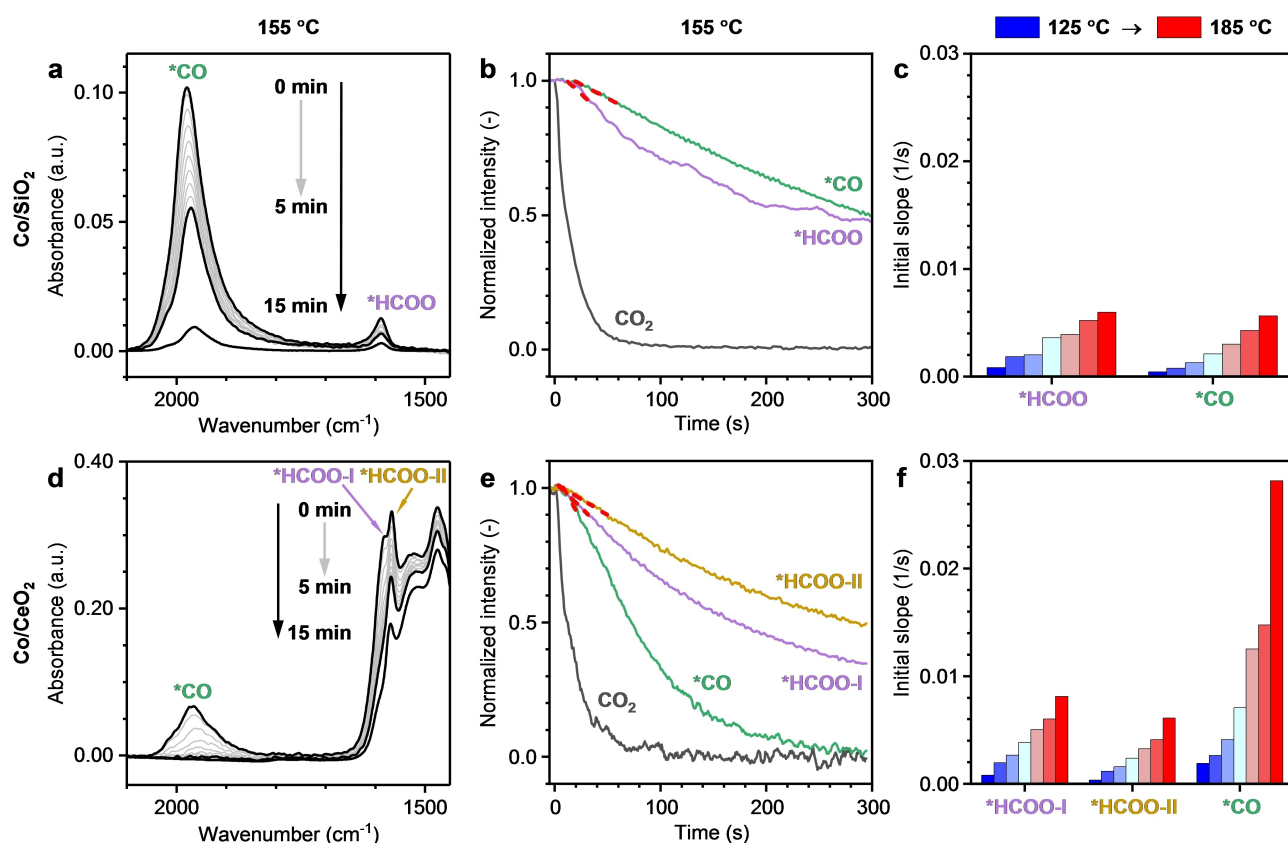

Figure 6. Operando transient kinetic step response FTIR on a)–c) Co/SiO_2 and d)–f) Co/CeO_2. a), d) $CO_2/H_2/He$ to H_2/He switch at 155°C. Black bold lines indicate scans acquired at 0, 5, and 15 minutes. Gray lines show the decay in species in the first 5 minutes. Carbonyls are labeled by *CO; formates by *HCOO. b), e) Normalized switch of Figure 6a and d, respectively, for carbonyls and formates at 155°C. Gaseous CO_2 (black) is given for comparison. Fitted initial slopes are indicated by red dashed lines. c), f) Initial slopes of the normalized decays for Co/SiO_2 and Co/CeO_2, respectively. Conditions: 0.6 mbar CO_2 and 200 mbar H_2 in He, total flow 200 mL min^{-1}, 125–185°C.

close to the coverages at steady-state (>90%). Thus, the initial rates provide qualitative information about the hydrogenation/decomposition rates of the species. The initial rate of disappearance of the formates is faster than that of the carbonyls for all switches over Co/SiO$_2$ (Figure 6c). The faster removal of the formates suggests that the formates precede the carbonyls in the reaction pathway.[25] To rule out a change in surface species coverages or surface changes as the main cause for the faster initial decomposition of formates compared to carbonyls on Co/SiO$_2$, a steady-state isotopic transient kinetic analysis (SSITKA) FTIR experiment was performed. In SSITKA, a switch between chemically identical feeds containing $^{12}CO_2$ and $^{13}CO_2$ isotopologues is made. Thus, in SSITKA-FTIR all spectra are acquired under steady-state. SSITKA-FTIR results at 175°C (Figure S28) demonstrated that the isotope exchange of formates precedes that of carbonyls, in line with the observations based on the transient kinetic step-responses. The step-response experiments on Co/CeO$_2$ demonstrate a faster decomposition of the carbonyls compared to Co/SiO$_2$. At 155°C, all the carbonyls were removed after 5 minutes on Co/CeO$_2$, while for Co/SiO$_2$ only 50% of them were removed (Figure 6d,e). Already at 125°C, approximately 50% of the carbonyls were removed after 5 minutes from Co/CeO$_2$ (only 10% for Co/SiO$_2$) (Figure S26d–f). It should be noted that the fast removal of carbonyls from Co/CeO$_2$ is not caused by their desorption as demonstrated by a control experiment in which the feed was rapidly changed to He instead of H$_2$/He (Figure S29). The initial rate of carbonyl conversion was up to 5 times higher on the ceria-supported catalyst (Figure 6f). As the carbonyl hydrogenation is slower than the decomposition of formates to carbonyls, the observed higher apparent rate of carbonyl hydrogenation on Co/CeO$_2$ defines the higher catalytic activity of this material.

The fast dynamics of both formates on Co/CeO$_2$ suggests that these species are active reaction intermediates. The step-response and SSITKA-FTIR experiments highlighted a difference in the transient behavior of the two different formates (Figure 6e and Figure S30). Formate-I exchanged faster than the red-shifted formate-II (Figure 6f). 2D correlation analysis confirmed this conclusion (Note S4). Therefore, formate-I is most likely the active formate in the dominant reaction pathway. Although the difference in nature of the two formates is not yet understood, it is hypothesized that these species are bound on different surface sites, e.g. the more active formate-I is at the Co-CeO$_2$ interface and formate-II on CeO$_2$, as previously proposed.[23,35,36,42]

Comparing formate-I on Co/CeO$_2$ to the formate species on Co/SiO$_2$, a faster transient behavior on Co/CeO$_2$ is observed. At a low temperature, formate-II is less dynamic than the formate on Co/SiO$_2$. However, upon increasing the temperature to 185°C this formate also decomposes faster than the formate on Co/SiO$_2$. Given the relatively large quantity of the formate-II species on Co/CeO$_2$ (Figure 5b), they can also contribute to the higher activity on Co/CeO$_2$, especially at higher temperatures. The reaction orders in CO$_2$ with respect to CH$_4$ at 175°C for Co/CeO$_2$ (Figure S31) are consistent with the effcient conversion of CO$_2$ to *CO

via *HCOO on Co/CeO$_2$. In contrast to Co/SiO$_2$, for which a shortage of reactive carbon species on the catalyst surface can be inferred from positive orders in CO$_2$, the orders for Co/CeO$_2$ are close to zero or even slightly negative (Figure S31). Carbon-containing species formed upon adsorption and activation of CO$_2$ on ceria (e.g., the observed carbonates and bicarbonates, absent on silica) can act as precursors to the reactive formates and carbonyls. This point is supported by step-response experiments at a higher partial pressure of CO$_2$ (25 mbar, Note S5 and Figure S32). The increased partial pressure of CO$_2$ leads to a significantly increased response time of the carbonyl and formate bands on Co/CeO$_2$, whereas for Co/SiO$_2$ the response was almost identical. Moreover, for Co/CeO$_2$ a sustained methane production was observed by mass spectrometry for ≈50 s after the switch to H$_2$, which was not observed for the Co/SiO$_2$ catalyst, lacking the adsorbed carbon-containing species necessary to sustain methane formation (Figures S6 and S33). In summary, CeO$_2$ provided a sufficient pool of active formates that on SiO$_2$ was much smaller. Moreover, significantly faster dynamics of carbonyls and formates on Co/CeO$_2$ compared to Co/SiO$_2$ explain the higher activity of the ceria-supported catalyst.

Conclusion

In this work, we demonstrated that Co/CeO$_2$ displays a superior low-temperature (<200°C) CO$_2$ methanation activity and selectivity at CO$_2$ partial pressures down to the current concentration of CO$_2$ in the atmosphere—0.4 mbar. The mechanistic origin of the unusual activity of Co/CeO$_2$ was studied by detailed spectroscopic investigations and compared to a conventional Co/SiO$_2$ catalyst. Reaction order studies and in situ NAP-XPS, point at the importance of the CeO$_2$ support and Co-CeO$_2$ interface in adsorbing and activating CO$_2$. In addition, our NAP-XPS data showcased the possibility of hydride formation on CeO$_2$ with deposited cobalt nanoparticles. The combination of steady-state, transient step-response, and SSITKA-FTIR experiments allowed for the identification of formates and carbonyls as the key reaction intermediates. Furthermore, an additional linear carbonyl species (C$_{ads}$-CO) was observed and, using 2D correlation analysis, linked to the facile CO dissociation on the catalyst surface. This C$_{ads}$-CO species can be used as a proxy for CO dissociation in future mechanistic studies. Our results point at a mechanism in which CO$_2$ is activated on the support and at the metal-support interface, leading to formates that further decompose into carbonyls. These carbonyls are subsequently hydrogenated to methane on the Co surface. We should note that we do not rule out a contribution of direct CO$_2$ dissociation at Co-CeO$_2$ interface to form carbonyls.[8] Hydrogen dissociation on the Co surface also leads to hydrogen spillover to the Co-ceria interface and ceria support to form formates and restore oxygen vacancies. Both the decomposition of formates to carbonyls and the hydrogenation of carbonyls to CH$_4$ were significantly faster on Co/CeO$_2$ than on Co/SiO$_2$. Moreover, the formate pool was much larger for the CeO$_2$-based

Angew. Chem. Int. Ed. **2023**, *62*, e202214864 (8 of 9)

© 2022 The Authors. Angewandte Chemie International Edition published by Wiley-VCH GmbH

catalyst. The combination of a higher concentration of active intermediates and the higher intrinsic activity of formates and carbonyls explains the high activity of Co/CeO_2 at low partial CO_2 pressures and low temperatures. These results emphasize the role of the metal-ceria interface in CO_2 hydrogenation chemistry and provide a foundation for the development of better catalysts for the utilization of CO_2.

Conflict of Interest

The authors declare no conflict of interest.

Data Availability Statement

The data that support the findings of this study are available from the corresponding author upon reasonable request.

[1] R. M. Cuéllar-Franca, A. Azapagic, *J. CO2 Util.* **2015**, *9*, 82–102.
[2] F. A. Rahman, M. M. A. Aziz, R. Saidur, W. A. W. A. Bakar, M. R. Hainin, R. Putrajaya, N. A. Hassan, *Renewable Sustainable Energy Rev.* **2017**, *71*, 112–126.
[3] P. A. U. Aldana, F. Ocampo, K. Kobl, B. Louis, F. Thibault-Starzyk, M. Daturi, P. Bazin, S. Thomas, A. C. Roger, *Catal. Today* **2013**, *215*, 201–207.
[4] M. A. A. Aziz, A. A. Jalil, S. Triwahyono, A. Ahmad, *Green Chem.* **2015**, *17*, 2647–2663.
[5] A. Álvarez, A. Bansode, A. Urakawa, A. V. Bavykina, T. A. Wezendonk, M. Makkee, J. Gascon, F. Kapteijn, *Chem. Rev.* **2017**, *117*, 9804–9838.
[6] J. Guilera, M. Filipe, A. Montesó, I. Mallol, T. Andreu, *J. Cleaner Prod.* **2021**, *287*, 125020.
[7] K. Ghaib, F.-Z. Ben-Fares, *Renewable Sustainable Energy Rev.* **2018**, *81*, 433–446.
[8] A. Parastaev, V. Muravev, E. Huertas Osta, A. J. F. Van Hoof, T. F. Kimpel, N. Kosinov, E. J. M. Hensen, *Nat. Catal.* **2020**, *3*, 526–533.
[9] T. Franken, A. Heel, *J. CO2 Util.* **2020**, *39*, 101175.
[10] Y. Yamazaki, M. Miyaji, O. Ishitani, *J. Am. Chem. Soc.* **2022**, *144*, 6640–6660.
[11] R. Sen, A. Goeppert, S. Kar, G. K. S. Prakash, *J. Am. Chem. Soc.* **2020**, *142*, 4544–4549.
[12] K. Wei, H. Guan, Q. Luo, J. He, S. Sun, *Nanoscale* **2022**, *14*, 11869–11891.
[13] F. Kosaka, Y. Liu, S.-Y. Chen, T. Mochizuki, H. Takagi, A. Urakawa, K. Kuramoto, *ACS Sustainable Chem. Eng.* **2021**, *9*, 3452–3463.
[14] T. W. Van Deelen, C. Hernández Mejía, K. P. De Jong, *Nat. Catal.* **2019**, *2*, 955–970.
[15] F. Wang, S. He, H. Chen, B. Wang, L. Zheng, M. Wei, D. G. Evans, X. Duan, *J. Am. Chem. Soc.* **2016**, *138*, 6298–6305.
[16] N. Daelman, M. Capdevila-Cortada, N. López, *Nat. Mater.* **2019**, *18*, 1215–1221.
[17] J. A. Farmer, C. T. Campbell, *Science* **2010**, *329*, 933–936.
[18] T. A. Le, M. S. Kim, S. H. Lee, E. D. Park, *Top. Catal.* **2017**, *60*, 714–720.
[19] T. H. Nguyen, H. B. Kim, E. D. Park, *Catalysts* **2022**, *12*, 212.
[20] K. Chang, H. Zhang, M. Cheng, Q. Lu, *ACS Catal.* **2020**, *10*, 613–631.
[21] A. Yu. Khodakov, J. Lynch, D. Bazin, B. Rebours, N. Zanier, B. Moisson, P. Chaumette, *J. Catal.* **1997**, *168*, 16–25.
[22] D. Song, J. Li, Q. Cai, *J. Phys. Chem. C* **2007**, *111*, 18970–18979.
[23] A. Paredes-Nunez, D. Lorito, N. Guilhaume, C. Mirodatos, Y. Schuurman, F. C. Meunier, *Catal. Today* **2015**, *242*, 178–183.
[24] G. N. Vayssilov, M. Mihaylov, P. St. Petkov, K. I. Hadjiivanov, K. M. Neyman, *J. Phys. Chem. C* **2011**, *115*, 23435–23454.
[25] X. Wang, H. Shi, J. Szanyi, *Nat. Commun.* **2017**, *8*, 513.
[26] A. Beck, M. Zabilskiy, M. A. Newton, O. Safonova, M. G. Willinger, J. A. van Bokhoven, *Nat. Catal.* **2021**, *4*, 488–497.
[27] H. Mansour, E. Iglesia, *J. Am. Chem. Soc.* **2021**, *143*, 11582–11594.
[28] W. Chen, B. Zijlstra, I. A. W. Filot, R. Pestman, E. J. M. Hensen, *ChemCatChem* **2018**, *10*, 136–140.
[29] G. Kadinov, C. Bonev, S. Todorova, A. Palazov, *J. Chem. Soc. Faraday Trans.* **1998**, *94*, 3027–3031.
[30] Z. Wu, Y. Cheng, F. Tao, L. Daemen, G. S. Foo, L. Nguyen, X. Zhang, A. Beste, A. J. Ramirez-Cuesta, *J. Am. Chem. Soc.* **2017**, *139*, 9721–9727.
[31] A. H. Clark, K. A. Beyer, S. Hayama, T. I. Hyde, G. Sankar, *Chem. Mater.* **2019**, *31*, 7744–7751.
[32] V. Muravev, G. Spezzati, Y.-Q. Su, A. Parastaev, F.-K. Chiang, A. Longo, C. Escudero, N. Kosinov, E. J. M. Hensen, *Nat. Catal.* **2021**, *4*, 469–478.
[33] C. Copéret, D. P. Estes, K. Larmier, K. Searles, *Chem. Rev.* **2016**, *116*, 8463–8505.
[34] A. Paredes-Nunez, D. Lorito, L. Burel, D. Motta-Meira, G. Agostini, N. Guilhaume, Y. Schuurman, F. Meunier, *Angew. Chem. Int. Ed.* **2018**, *57*, 547–550; *Angew. Chem.* **2018**, *130*, 556–559.
[35] L. Falbo, C. G. Visconti, L. Lietti, J. Szanyi, *Appl. Catal. B* **2019**, *256*, 117791.
[36] M. Marwood, R. Doepper, A. Renken, *Appl. Catal. A* **1997**, *151*, 223–246.
[37] A. Karelovic, P. Ruiz, *J. Catal.* **2013**, *301*, 141–153.
[38] T. Lear, R. Marshall, J. Antonio Lopez-Sanchez, S. D. Jackson, T. M. Klapötke, M. Bäumer, G. Rupprechter, H.-J. Freund, D. Lennon, *J. Chem. Phys.* **2005**, *123*, 174706.
[39] S.-C. Lee, J.-H. Jang, B.-Y. Lee, J.-S. Kim, M. Kang, S.-B. Lee, M.-J. Choi, S.-J. Choung, *J. Mol. Catal. Chem.* **2004**, *210*, 131–141.
[40] S. Eckle, H.-G. Anfang, R. J. Behm, *J. Phys. Chem. C* **2011**, *115*, 1361–1367.
[41] T. Gott, S. T. Oyama, *J. Catal.* **2009**, *263*, 359–371.
[42] X. Wang, Y. Hong, H. Shi, J. Szanyi, *J. Catal.* **2016**, *343*, 185–195.